Supplementary Information

Synthesis, structural insights, biological screening of DNA targeted Ru(II)(*η*6-*p*-cymene) complexes containing bioactive amino-benzothiazole ligand scaffolds

Suffora Akhter [a], Abdur Rehman [b], S.M.A.Abidi [b], Farukh Arjmand [a] and Sartaj Tabassum [a]*

*[a] *Department of Chemistry, Aligarh Muslim University, Aligarh, 202002*

[b] *Section of Parasitology, Department of Zoology, Aligarh Muslim University, Aligarh, India*

**Email: tsartaj62@yahoo.com, 9358255791*

Experimental section

Materials and instrumentation

All reagents, 2-Amino-4-cholorobenzothiazole, 2-Amino-6-fluorobenzothiazole and [Ru(η^6-*p*-cymene)Cl_2]$_2$, Ethidium bromide(EB) and Tris-(hydroxymethyl)aminomethane(Tris-buffer), were purchased from Sigma Aldrich. Ct-DNA and BSA was purchased from Sigma Chemicals.co and stored at 4 ˚C. All other solvents were obtained from Merck and used as such without further purification. The interaction studies of ct-DNA, were carried out in tris buffer (5.0 mM Tris-HCl, 50.0 mM NaCl, pH=7.4). Fourier-Transform infrared (FT-IR) spectra were recorded on Perkin Elmer FT-IR spectrometer in the 4000-400 cm^{-1} range with KBr. The **^{1}H**-NMR and **^{13}C**-NMR were recorded on Joel Spectrometer. ESI-MS spectra were recorded on a Micromass Quattro II triple quadrupole mass spectrometer. PerkinElmer Lambda 25 was used to record electronic spectra using cuvettes of 1cm path length. Emission spectra were obtained on Shimadzu RF-5301 PC spectrofluorometer. Circular dichroism (CD) measurements were carried on Jasco J-815-CD spectropolarimeter using 1 cm quartz cuvette. Cyclic voltammetry was carried out at CH instrument electro-chemical analyzer. SEM micrographs were recorded with a JEOL JSM-6510LV scanning electron microscope. Electrophoretic assays were carried out in Tris-borate-ethylenediaminetetraacetic acid buffer at 50 Vcm^{-1} visualized using UV Transilluminator.

Molecular docking studies were performed using HEX 8.0 software[1] which is an interactive molecular graphics program for calculating and displaying feasible docking modes of biomolecules. Autodock software was also used. Visualization of the docked pose was achieved using the Discovery Studio molecular graphics program.[2] The DFT studies were performed using Spartan 18V1.4.5(2019) version programme.[3]

Single crystal X-ray data were collected at 100 K by using the Bruker SMART APEX CCD diffractometer on graphite monochromatic MoK radiation (0.71073). The International Table for X-ray crystallography applied to the linear absorption coefficient, scattering factors for the atoms and anomalous dispersion correction. The data integration and reduction were worked out with SAINT software. For the collected reflections with SADABS, empirical absorption correction was applied and the space group was defined using XPREP. Only a few H atoms could be located in the difference Fourier maps in the structure. The remaining were positioned in calculated positions using idealized geometries (riding model) and assigned fixed isotropic displacement parameters. All non-H atoms were refined anisotropically.

Collection and *in-vitro* treatment of adult *Fasciola gigantica* worms

Adult worm of tropical liver fluke, *F. gigantica,* were collected from the naturally infected Indian water buffalo, *Bubalus bubalis* slaughtered at the local abattoir. The worms were washed thoroughly with Hanks' balanced salt solution (HBSS) and given a quick rinse in HBSS containing Penicillin-Streptomycin followed by multiple washes in HBSS.[4] The *in-vitro* effects of complexes **1** and **2** on the adult *F. gigantica* worms were investigated by incubating a total of 5 worms in 25 ml RPMI-1640 medium containing different concentrations (5-40 mg/ml) of each complex at 37 ± 1°C along with negative controls incubated in RPMI medium alone with out the test complexes. A batch of worms was treated with the known fasciolocidal drug, triclabendazole (TCBZ) at a concentration of 15 mg/ml.[5] After 6 h of incubation, the worms were removed, quickly washed with phosphate buffered saline and used for various studies. A

10 % (w/v) homogenate of the worms was prepared in 100 mM Tris-HCl buffer, pH 7.4 followed by centrifugation at 12,000 g for 30 min at 4 °C. The clear supernatant was collected and stored in aliquot at −80 °C until used. The protein content in each sample was estimated following the method of Spector (1978) using bovine serum albumin as standard.

Observation on parasite motility

The motility of the adult *F. gigantica* worms was visually recorded in the presence and absence of the test complexes and TCBZ. The worm motility was recorded at and interval of 60 min until the termination of the experiment. The motility was quantitatively expressed on a scale of 0-5 as described earlier [6] where 5 denotes highly active worms, 4 reflect active worms, 3 means slow movement throughout the body, 2 denotes motility only at ends of the worms, 1 denotes movement in flukes only when prodded and 0 for completely immotile worms.

Effect of *in-vitro* treatment on glutathione-S-transferase (GST) activity

The changes in the GST activity of adult *F. gigantica* worms was measured according to the method as described earlier.[7] The enzyme activity was expressed as units/mg protein using molar extinction coefficient of $9.6 \times 10^3\ M^{-1}cm^{-1}$.

Effect of in vitro treatment on superoxide dismutase (SOD) activity

The SOD activity in the treated and control flukes was measured according to the method of Marklund and Marklund (1974) with some minor modifications as described earlier.[6] The specific SOD activity was expressed as units/mg protein and one unit of SOD is defined as the amount of enzyme required to inhibit the autoxidation of pyrogallol by 50 % under the specified assay condition.

Estimation of lipid peroxidation

The amount of malondialdehyde (MDA) a byproduct formed as a result of lipid peroxidation process occurring during the oxidative stress was measured in control and treated samples following the method of Buege and Aust (1978).[8] The MDA level was expressed as n moles of

MDA formed/mg protein using molar extinction co-efficient of $1.56 \times 10^5\ M^{-1}cm^{-1}$ for MDA-tribarbituric acid adduct.

Determination of protein carbonylation

The level of protein carbonyls (PC) in the treated and untreated samples was determined according to the method of Levine et al. (1990).[9] The PC content in the samples were expressed as n moles of dinitrophenylhydrazine (DNPH) incorporated/mg protein, using $22{,}000M^{-1}cm^{-1}$ as the molar extinction coefficient.

Ultrastructural changes in the in vitro treated adult *Fasciola gigantica* worms

Scanning electron microscopy (SEM) was performed to study the ultrastructural changes in the tegument of the adult *F. gigantica* worms according to the procedure as described earlier. Briefly, the treated and control worms were flat fixed in 4% (w/v) glutaraldehyde buffered with 100mM sodium cacodylate solution (pH 7.4) containing 3% (w/v) sucrose. There after, the worms were rinsed with sodium cacodylate buffer. The specimens were dehydrated in ascending grades of ethanol, critically dried, sputter coated with gold and viewed on scanning electron microscope (JSM 6510LV, JOEL) maintained at the University Sophisticated Instruments Facility, Aligarh Muslim University, Aligarh.

Statistical analysis

The statistical analysis was performed using GraphPad software to determine the level of significance following one way ANOVA post hoc Tukey's test. Atleast three biological and technical replicates were included in each experiment. The results are presented as mean ± S.E.M. and p value <0.05 was considered statistically significant

Synthesis

Synthesis of complex **1**

In a round bottom flask, 612 mg of $[Ru(\eta^6\text{-}p\text{-cymene})Cl_2]_2$dimer (1 mmol) was dissolved in hot methanol and 369 mg of 2-Amino-4-cholorobenzothiazole (2 mmol) was added to it. The

reaction mixture was stirred for 6 hours till reddish brown product separated out. The product was dissolved in methanol and kept at undisturbed place for crystallization.

$[C_{17}H_{19}Cl_3N_2RuS]$, Yield: 71%, Melting point: 210 ˚C, FT-IR(KBr, υ_{max}/cm^{-1}): 3221.0 υ(–NH), 2966 υ(–CH_2), 1610.0 υ(–C=N), 786 υ(–C–Cl), 406 υ(Ru–Cl). **^{1}H-**NMR(500MHz, DMSO, δ, ppm): 10.9(s,1H), 7.74(s,1H), 7.58(d,1H), 7.57(d,1H), 6.99(t,1H), 5.76(d,2H), 5.71(d,2H), 2.81(m,1H), 2.48(s,3H), 1.18(d,6H) . **^{13}C**-NMR(100MHz, DMSO, *δ*, ppm): 167.7, 149.5, 132.4, 120.6, 100, 107, 85.5$(C_2)_{cym}$, 86.7$(C_6)_{cym}$, 40, 30.3$(CH)_{cym}$, 18.26$(CH_3)_{cym}$. ESI-MS(*m/z*):490, 182 ; UV-vis(1×10^{-4}M,Methanol,λ/nm) : 265, 227.

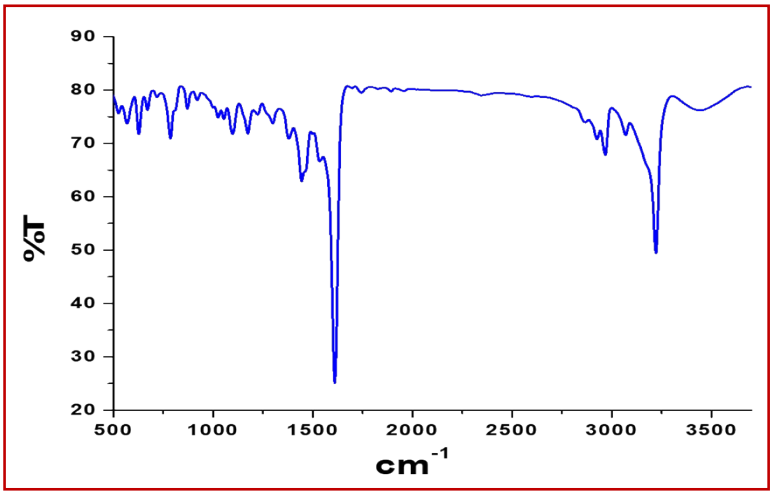

Fig.S1 FT-IR spectrum of Complex **1**

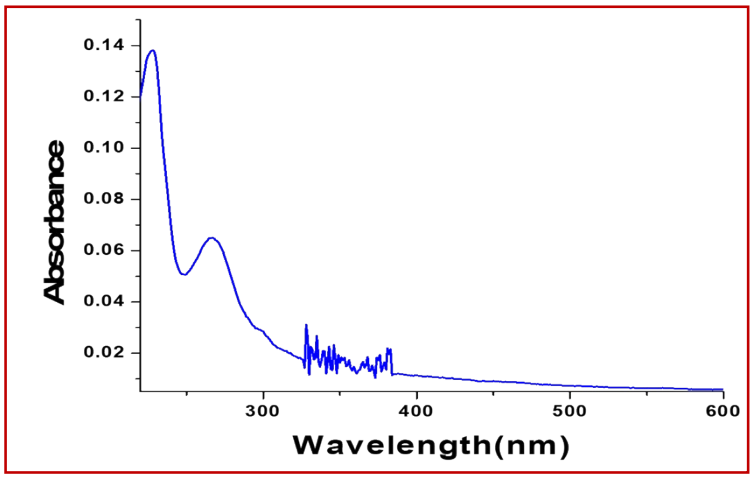

Fig. S2 UV-vis spectrum of Complex **1**

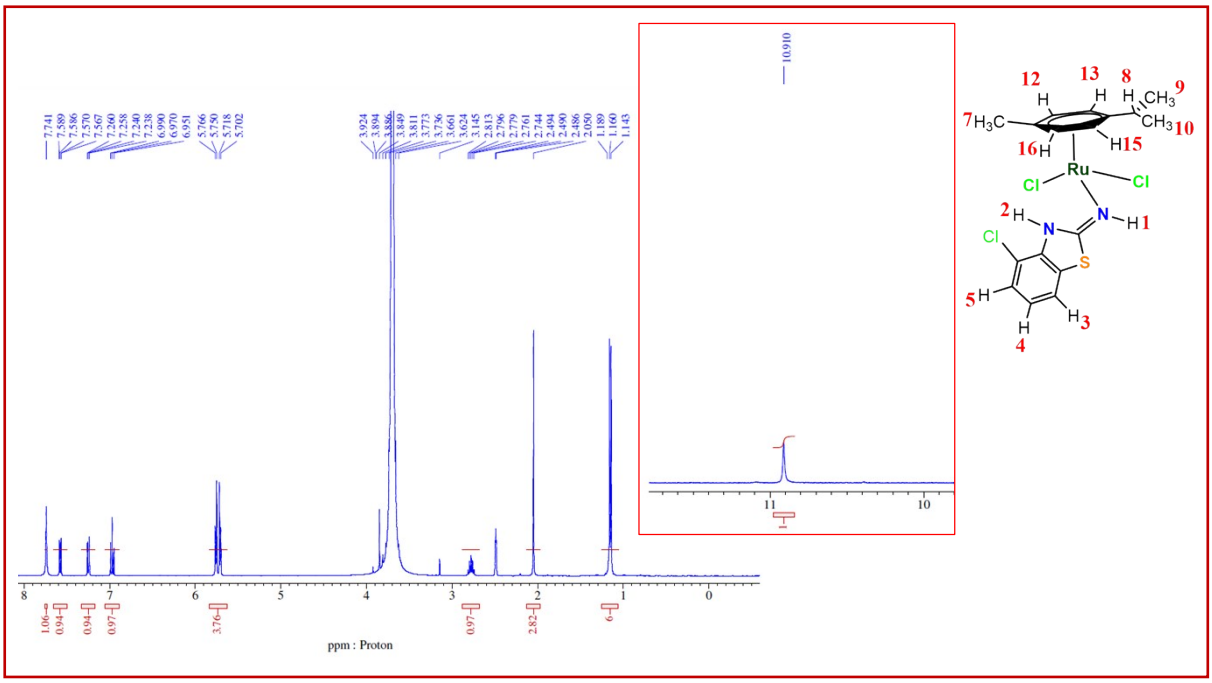

Fig. S3 ^{1}H-NMR spectrum of Complex **1**

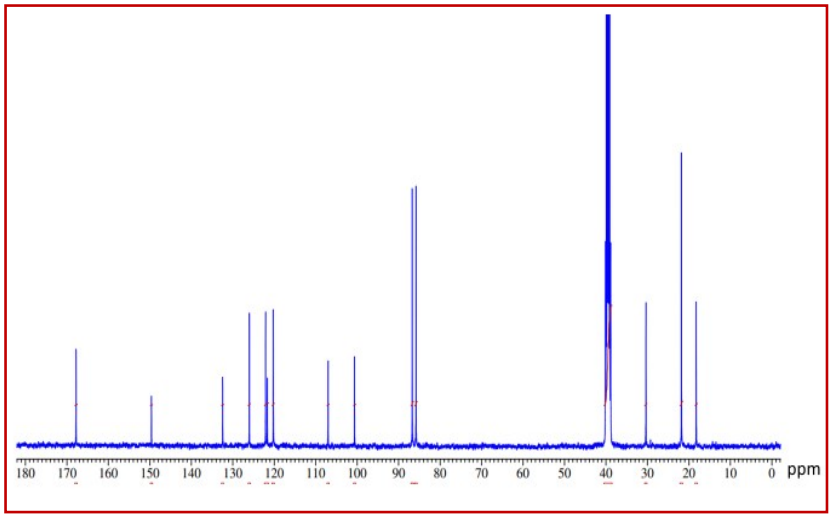

Fig. S4 ^{13}C-NMR spectrum of Complex **1**

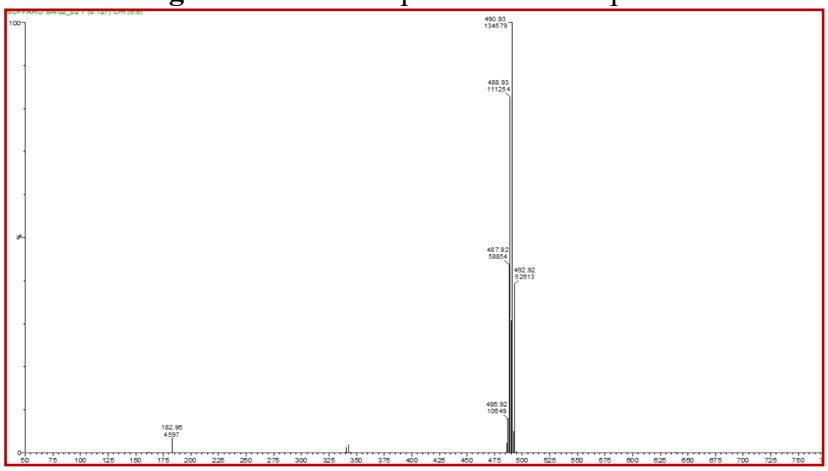

Fig. S5 **ESI-MS** spectrum of Complex **1**

Synthesis of complex **2**

To a mixture of 612 mg of [Ru(η^6-*p*-cymene)Cl_2]$_2$dimer (1 mmol) dissolved in hot methanol 336 mg of 2-Amino-6-fluororobenzothiazole (2 mmol) was added in a round bottom flask. The reaction mixture was stirred for 24 hours and filtered in a beaker and kept undisturbed for crystallization. After 4 days reddish brown crystals of complex **1** were obtained.

[$C_{17}H_{19}Cl_2FN_2RuS$], Yield: 67.5%, Melting point: 143 ˚C, FT-IR(KBr, υ_{max}/cm^{-1}): 3433-3119.0 υ (–NH_2), 2926 υ (–CH_2), 1612.0 υ (–C=N),1462 υ (–C–F), 406 υ (Ru–Cl). **^{1}H**-NMR(500MHz, DMSO, δ, ppm): 7.50(s,2H), 7.52(d,1H), 7.50(t,1H), 7.2(d,1H), 5.7(d,2H), 5.6(d,2H), 2.7(m,1H), 2.04(s,3H), 1.18(d,6H) . **^{13}C**-NMR(100MHz, DMSO, δ, ppm): 166, 156, 158, 149,132, 118, 108, 100, 85.82$(C_2)_{cym}$, 86.7$(C_6)_{cym}$, 40.13, 30.3$(CH)_{cym}$, 18.22$(CH_3)_{cym}$ **^{19}F**-NMR(100MHz, , δ, ppm) -122.5 ; ESI-MS(*m/z*): 474, 472 ; UV-vis(1×10^{-4}M,Methanol,λ/nm) : 223, 259.

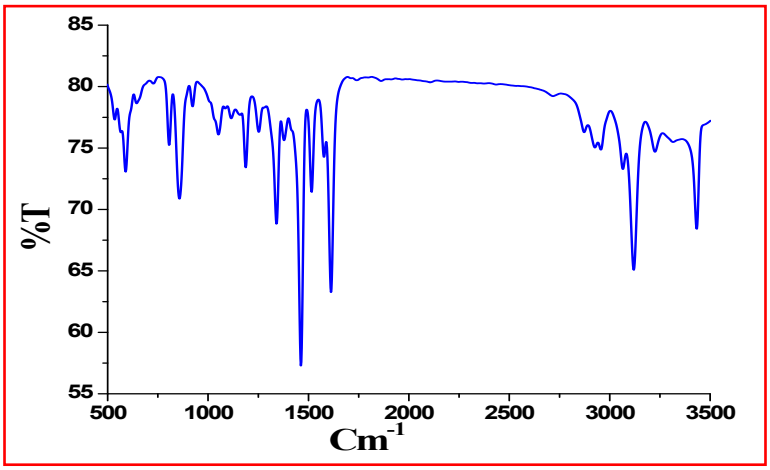

Fig.S6 FT-IR spectrum of Complex **2**

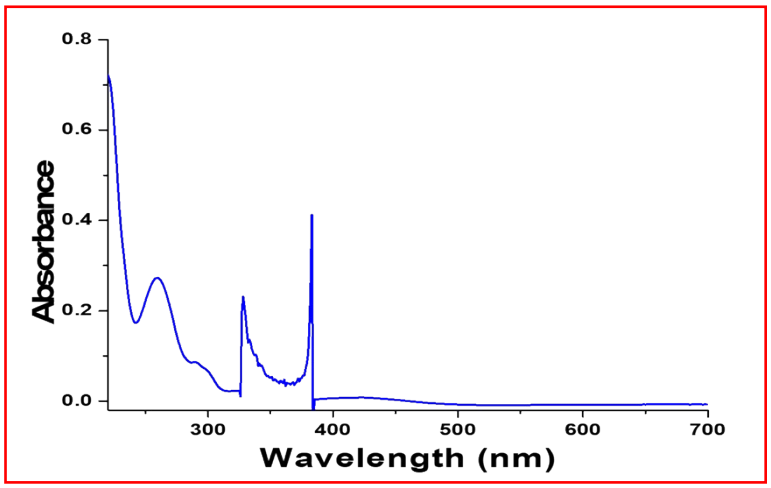

Fig. S7 UV-vis spectrum of complex **2**.

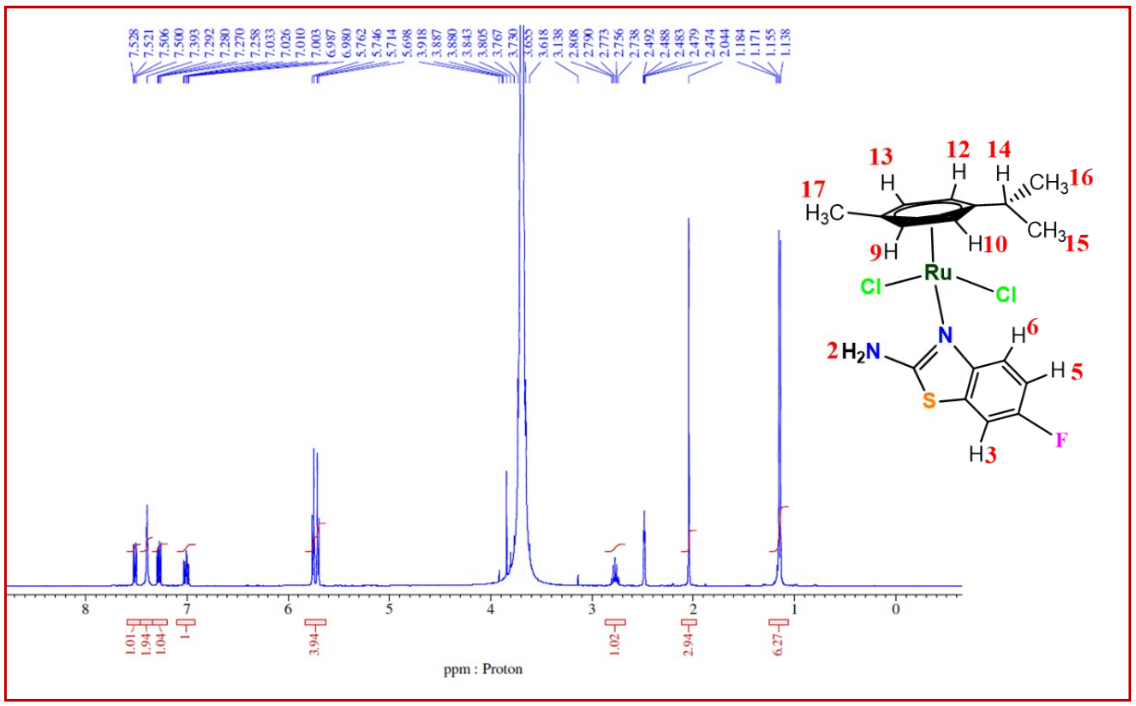

Fig. S8 ^{1}H-NMR spectrum of Complex **2.**

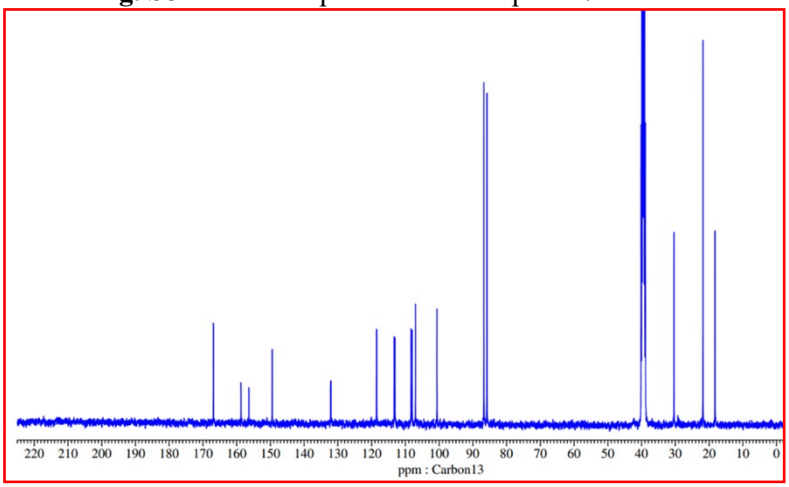

Fig. S9 ^{13}**C**-NMR spectrum of Complex **2.**

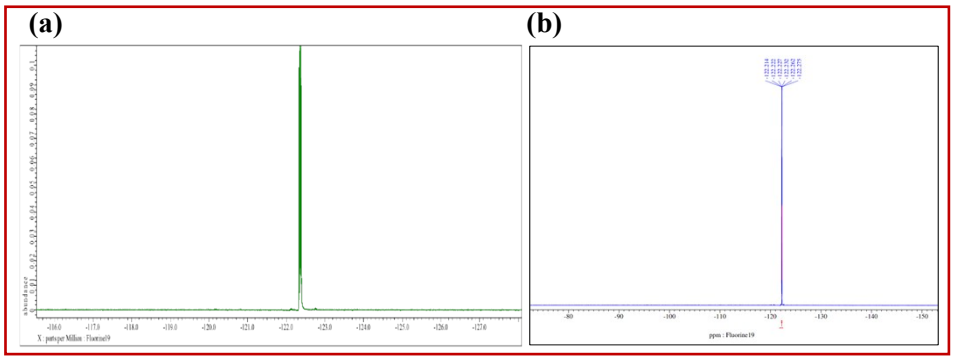

Fig. S10 ^{19}**F**-NMR spectrum of (a) Complex **2** and (b) 2-Amino-6-fluorobenzothiazole

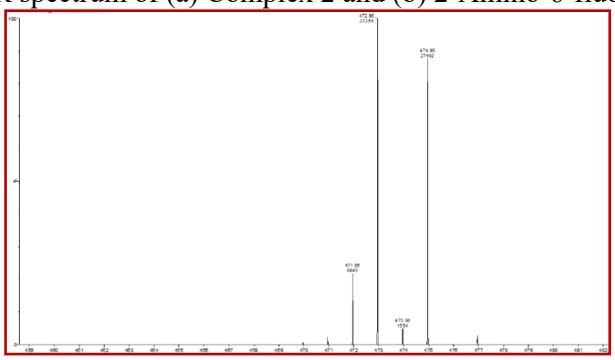

Fig. S11 ESI-MS spectrum of Complex **2**

Table S1. Crystal and structure refinement data of complex 1 and 2.

Identification code	Complex **1**	Complex **2**
Empirical formula	$[C_{17}H_{19}Cl_3N_2RuS]$	$[C_{17}H_{19}Cl_2FN_2RuS]$
Formula weight	490.82	474.37
Temperature/K	298K	298K
Crystal system	Orthorhombic	Monoclinic
Space group	*Pna2$_1$*	*P21/n*
a/Å	17.47(2)	13.49(3)
b/Å	11.18(2)	7.38(2)
c/Å	9.71(1)	21.95(6)
α/°	90	90
β/°	90	105.3
γ/°	90	90
Volume/Å^3	1898.16(4)	2109.9(10)
Z	4	4
ρ_{calc} Mg/m^3	1.717	1.493
μ/mm^{-1}	1.36	1.105
F(000)	984.0	952.0
Radiation	MoKα(λ=0.710)	MoKα(λ=0.710)
Independent reflections	4133	4588
Goodness-of-fit on F^2	0.996	1.035

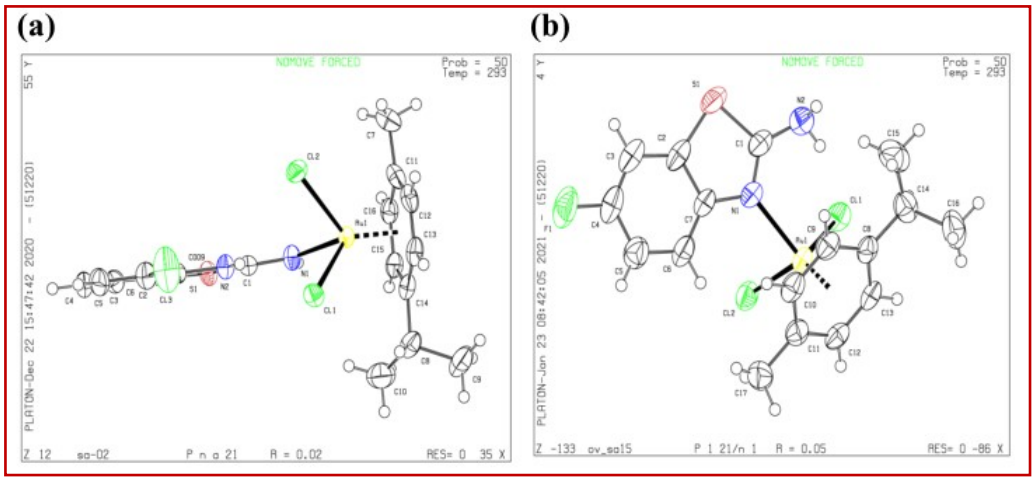

Fig. S 12 Structure of Complex **1** and Complex **2**.

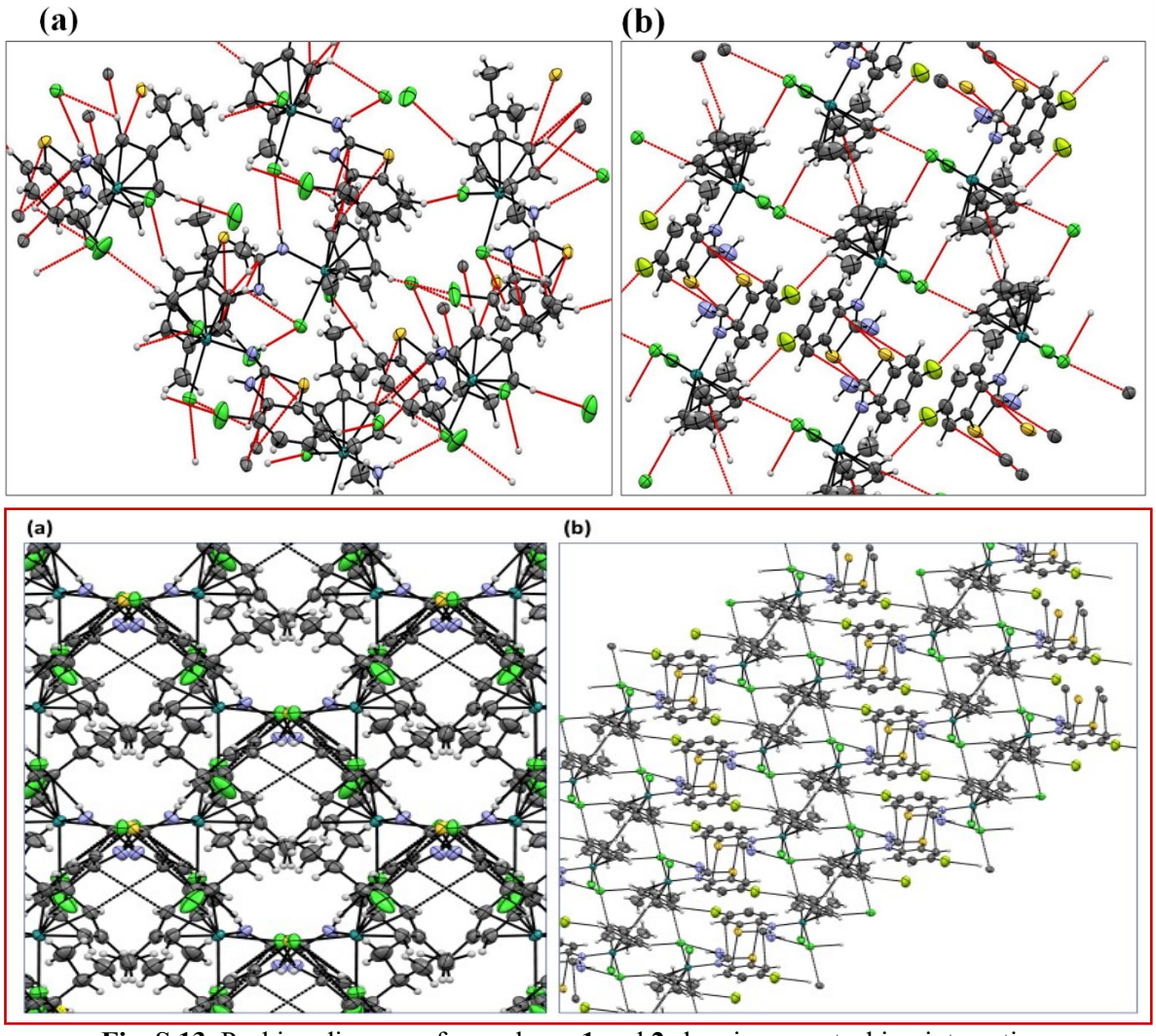

Fig. S 13. Packing diagram of complexes **1** and **2** showing π-π stacking interaction.

Table S2. Comparision of observed and calculated bondlenths of complex 1 and 2

Complex 1 (Å)			**Complex 2 (** Å)		
Bond Type	SC XRD	DFT	Bond Type	SC XRD	DFT
N2-H2	0.860	0.810	N2-C1	1.349	1.334
N2-C1	1.358	1.320	N2-H2A	0.867	0.867
N1-C1	1.285	1.564	N2-H2B	1.349	0.838
N1-H1	0.67	0.882	N1-C1	1.311	1.168
Ru1-N1	2.113	2.113	Ru1-N1	2.170	2.169
Ru-Cl1	2.434	1.064	Ru-Cl1	2.430	1.079
Ru-Cl2	2.443	1.091	Ru-Cl2	2.435	1.109

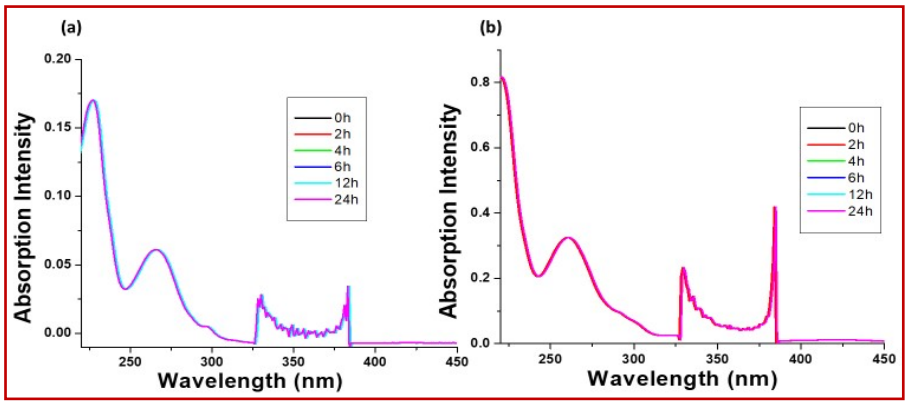

Fig.S14 Absorption spectra of Complex **1**(a) and complex **2** (b) in aqueous saline Tris-HCl buffer at different time intervals

Hirshfeld surface analysis

To expound the space occupied by a molecule in a crystal, Hirshfeld surface analysis was performed. This analysis utilizes the definition of an atom fragment in a compound and hence the atomic charge and other properties are obtained by numerical interactions and help us to predict and quantify the shape and size of molecules. The Hirshfeld surfaces of complexes **1** and **2** are displayed in S15. The distance to the nearest atoms outside, d_e and d_i are used to explore the C–H---π, and H--H etc interactions and they also give an idea about the proximity of intermolecular contacts in a crystal. The distance d_i and d_e mapped on the Hirshfeld surface

were further used to generate the fingerprint plots. The normalised contacts, d_{norm}, are shown in a red-white-blue colour scheme, with red emphasising shorter contacts, white emphasising contacts near the *Vdw* separation, and blue emphasising extended contacts.

Fingerprint plots highlight specific close contacts and allow for quick comparison of the same or different crystals. Hirshfeld surface area due to C–H (C–H ···π) and C–C(π ···π), H–Cl and N–H interactions are shown in Fig. S16. From the studies it emerged that complex **1** has the dominating interactions of H–Cl(28.9%) and C–H(13.5%) and complex **2** has the dominating interactions of Cl–H(17.8%), H–F(9.8%) and C–H (4.5%). The other interactions that stabilize the crystal are the N–H and C–C interactions.

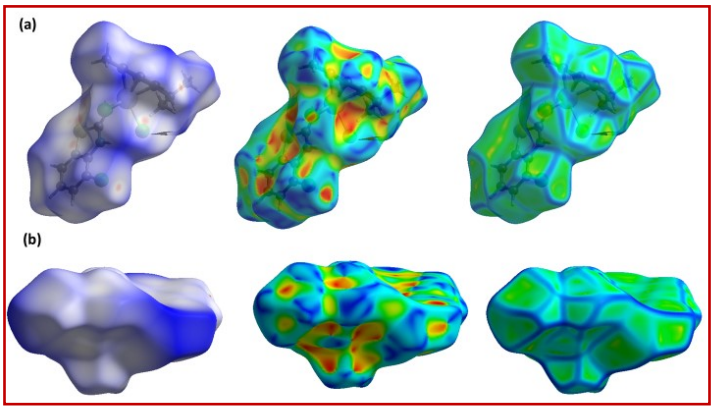

Fig.S15. Hirshfeld surface of complexes **1** (a) and **2** (b) mapped with d norm , shape index and curvedness .

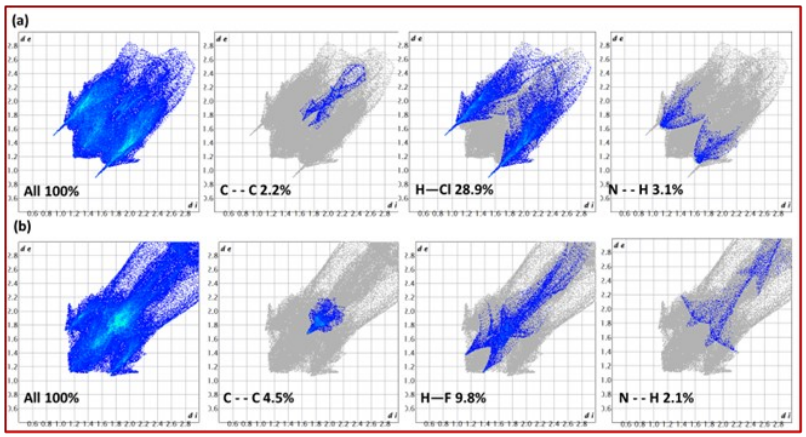

Fig.S16. Fingerprint plots for (a) complex **1** and (b) complex **2**

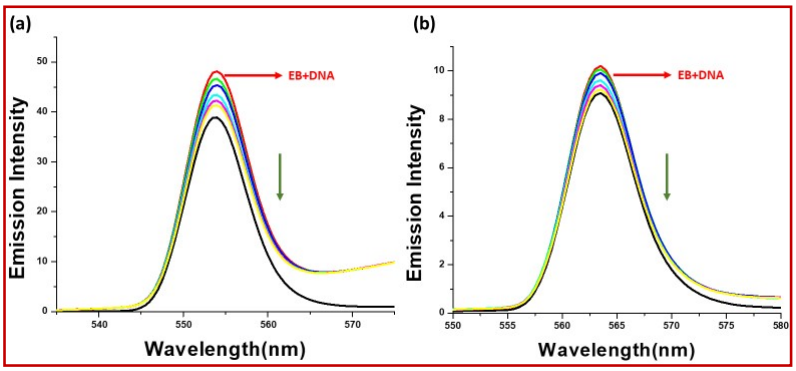

Fig. S17. Emission spectra of (a) complex **1** (b) complex **2** in aqueous saline Tris-HCl buffer.

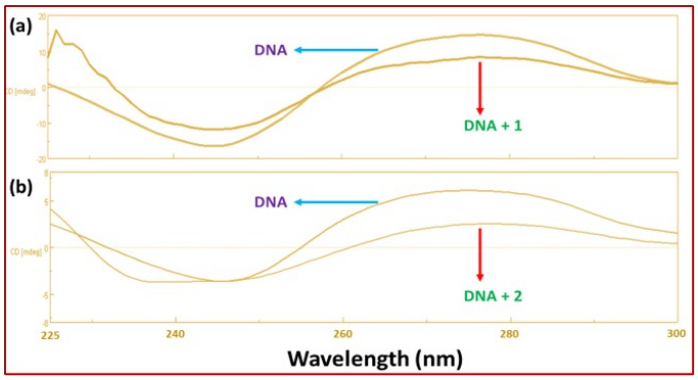

Fig. S18. CD spectra of ct-DNA alone and in presence of complex **1** and complex **2.**

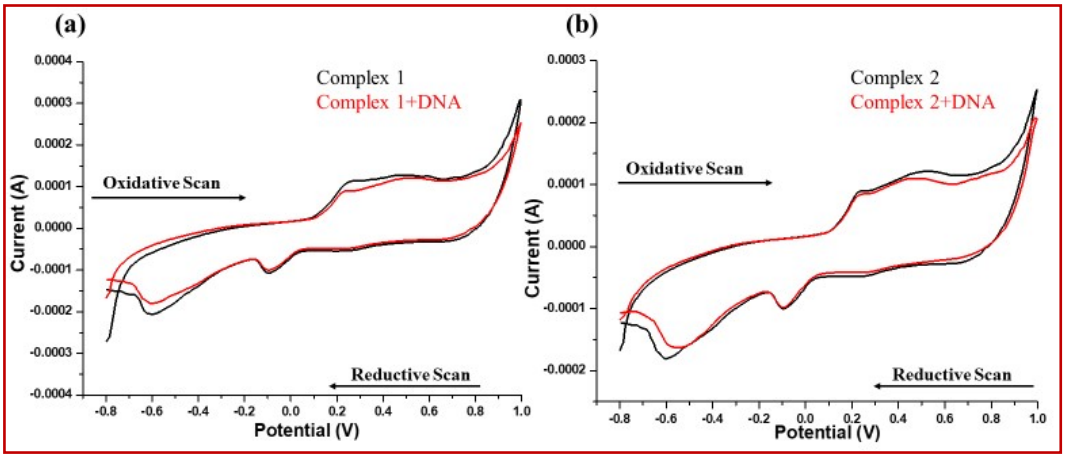

Fig. S19. Cyclic voltammogram of complex **1** and **2** in aqueous saline Triss-HCl buffer at the scan rate of 0.1 Vs^{-1}.

Protein Binding

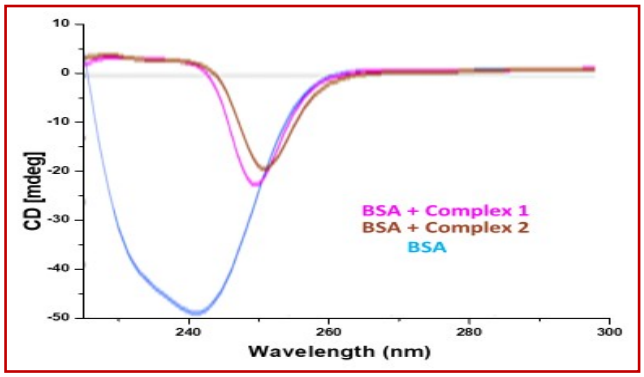

Fig. S20. CD spectra of complex **1** and **2** with BSA

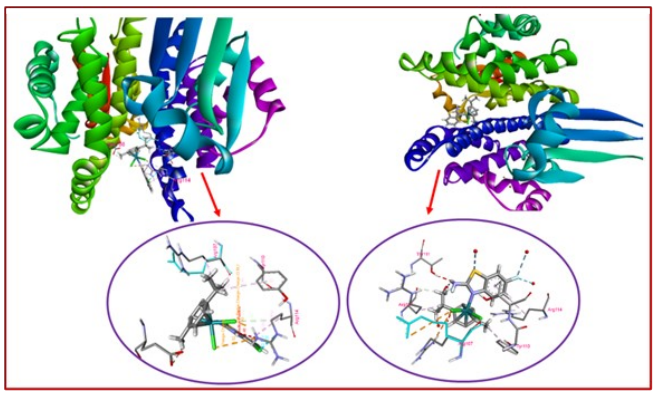

Fig.S21. Favourable binding positions of complex **1** and complex **2** with GST**.**

Docking With H.contortus β tubulin

Hex software was used to Dock the TCBZ, complexes **1** and **2** with the Tubulin model (PDB ID 1OJ0) and the results were compared. 1OJ0 is a model of H.contortus β tubulin bound to albendazole sulphoxide. This is a theoretical model Released on 2003 by Robinson et al.

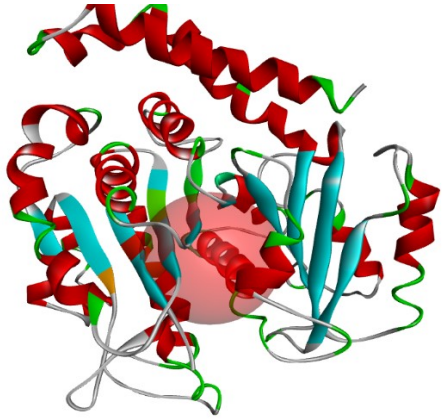

Fig. S22. Favourable binding sites of the 1OJ0 as shown by the Maroon sphere.

TCBZ binds in the favourable binding region and interacts with the amino acids val A255, arg A251, lys A252 and cys A129. Both the complexes **1** and **2** bind in the same region where TCBZ interacts that is in close vicinity of the amino acids leu A361, val A231, phe A270, gly A360 etc. One conventional hydrogen bond is found between sulphur of amino benzothiazole and asn A247 amino acid of the β-tubulin. The greater the negative binding energy values, the greater is the binding propensity of the drug towards the molecule. Hence TCBZ (-223.62 KJ mol^{-1}) > 2 (-172.01 KJ mol^{-1}) > 1 (-167.01 KJ mol^{-1}).

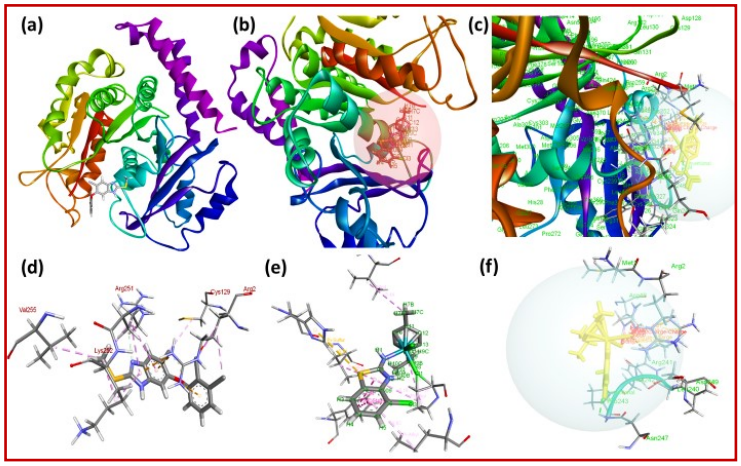

Fig.S23. Favourable binding positions of TCBZ (a, d) , 1(b, e) and 2 (c, f).

Docking Studies with β-tubulin PDB ID : 1tub

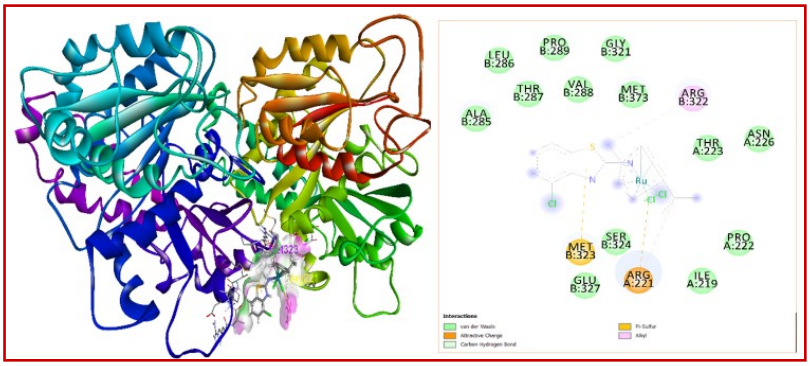

Fig. S24. Favourable binding posses of complex **1**.

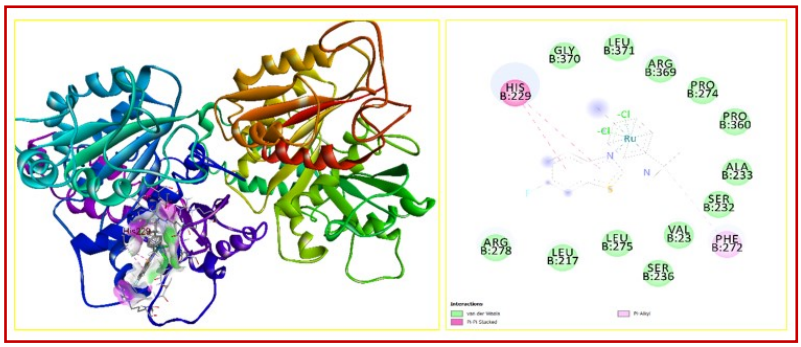

Fig. S25. Favourable biding posses of complex **2**.

Anthelmentic Activity

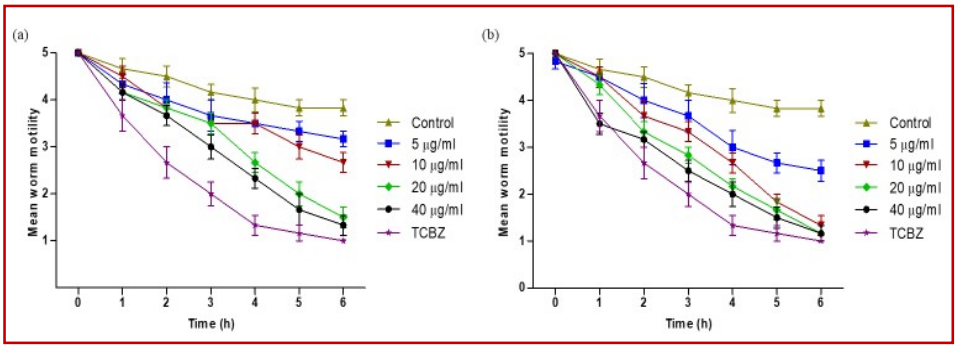

Fig. S26. Time and concentration-dependent changes in the motility of adult worms upon treatment with complex **1** (a) and complex **2** (b).

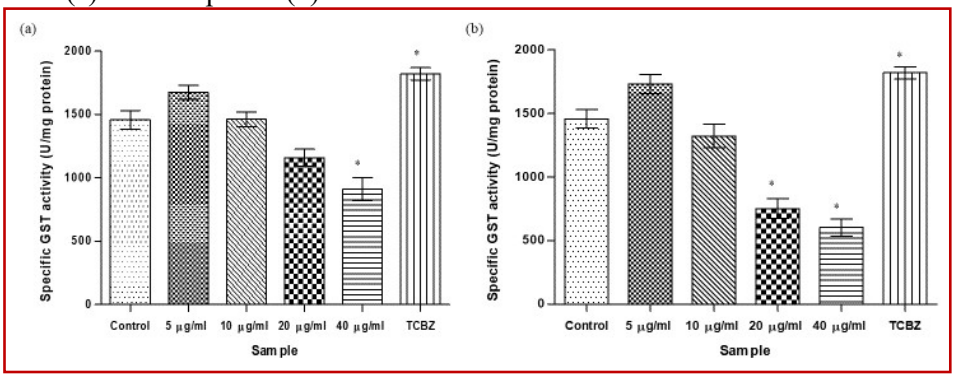

Fig. S27. The changes in the level of Glutathione-S-transferase (GST) in adult *Fasciola gigantica* post treatment with different concentrations of complex **1** (a) and complex **2** (b).

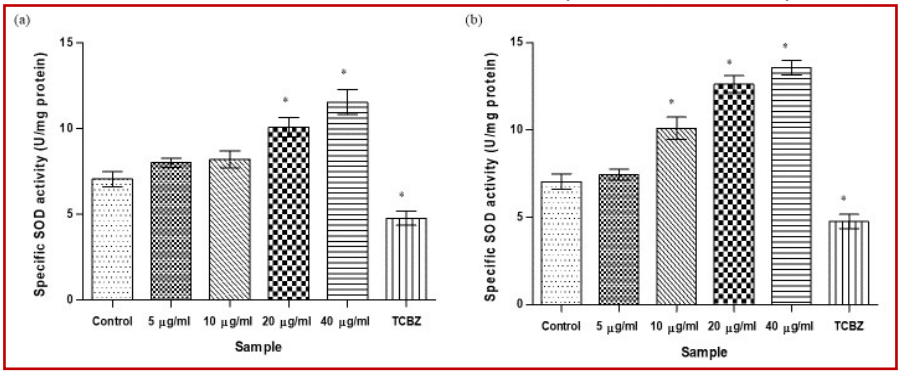

Fig. S28. The changes in the superoxide dismutase (SOD) activity in adult *Fasciola gigantica* treated with different concentrations of complex **1** (a) and complex **2** (b)

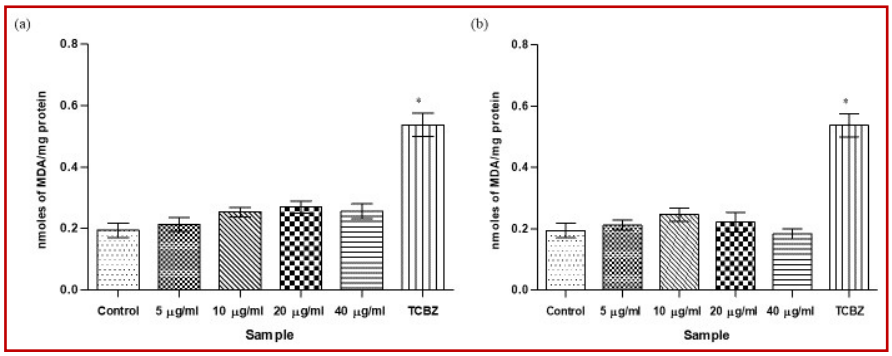

Fig. S29. The changes in the level of malondialdehyde (MDA) in adu1t *Fasciola gigantica* treated with different concentrations of of complex **1** (a) and complex **2** (b)

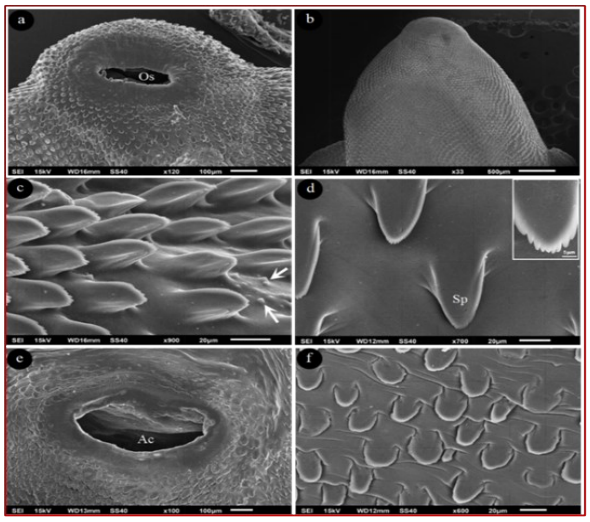

Fig. S30. Representative scanning electron micrographs of the control adult *Fasciola gigantica* worms. The anterior region bearing oral sucker with concentrically arranged spines (a), dorsal surface of the worm covered with spines (b), intact spines located on the anterior-lateral region of the ventral surface (c) having clusters of papillae (arrow), backwardly pointing spines on the ventral surface with inset showing the serrated spine (d). The main attachement organ acetablum with acetabular opening (e) and numerous spines present on dorsal surface (f). Os: Oral sucker, Sp: Spine, Ac: Acetabulum.

References

1 G. Macindoe, L. Mavridis, V. Venkatraman, M. D. Devignes and D. W. Ritchie, *Nucleic Acids Res.*, 2010, **38**, 445–449.

2 Free Download: BIOVIA Discovery Studio Visualizer - Dassault Systèmes, https://discover.3ds.com/discovery-studio-visualizer-download, (accessed 12 June 2021).

3 Spartan Software, Inc., https://www.spartansoftwareinc.com/, (accessed 12 June 2021).

4 P. A. A. Shareef, G. P. Brennan, P. McVeigh, M. A. H. Khan, R. M. Morphew, A.

Mousley, N. J. Marks, M. K. Saifullah, P. M. Brophy, A. G. Maule and S. M. A. Abidi, *Acta Trop.*, 2014, **136**, 108–117.

5 U. Duthaler, T. A. Smith and J. Keiser, *Antimicrob. Agents Chemother.*, 2010, **54**, 4596–4604.

6 A. Rehman, R. Ullah, I. Uddin, I. Zia, L. Rehman and S. M. A. Abidi, *Exp. Parasitol.*, 2019, **198**, 95–104.

7 W. H. Habig, M. J. Pabst, G. Fleischner, Z. Gatmaitan, I. M. Arias and W. B. Jakoby, *Proc. Natl. Acad. Sci. U. S. A.*, 1974, **71**, 3879–3882.

8 J. A. Buege and S. D. Aust, *Methods Enzymol.*, 1978, **52**, 302–310.

9 A. S. Bayer, V. J. Scott and L. B. Guze, *Semin. Arthritis Rheum.*, 1979, **9**, 66–74.